Acta Crystallographica Section A
Foundations of Crystallography
ISSN 0108-7673

Received 9 April 2004
Accepted 14 June 2004

X-ray standing waves in a heterostructure: application to a $Zn_{1-x}Co_xO$ epilayer on $ZnO(00.\bar{1})$–O substrate

Y. Zheng,* J. C. Boulliard, A. Soyer and J. F. Pétroff

Laboratoire de Minéralogie–Cristallographie, Universités Pierre et Marie Curie (Paris VI) et Paris VII, CNRS UMR 7590, Case 115, 4 place Jussieu, 75252 Paris CEDEX 05, France. Correspondence e-mail: zheng@lmcp.jussieu.fr

X-ray standing waves (XSW) in a thin epitaxic film are treated in the framework of the dynamical theory. It is demonstrated that the fluorescence yield around the main peak of the rocking curve has essentially the same characteristics as that of the usual XSW on a bulk crystal surface. Thus, XSW provide a direct method to probe the atom position in a thin film. The method was applied to an epilayer of the diluted magnetic semiconductor $Zn_{0.94}Co_{0.06}O$, in order to determine the Co-atom position. The XSW established that Co atoms occupy the substitutional Zn site in the ZnO matrix, although their coherent fraction, which measures the degree of order, is rather low. Moreover, the measurement of the Zn fluorescence in the film gives approximately the same value for the coherent fraction of the Zn atoms. Besides, by using the substrate rocking curve, it is shown that the XSW signal of the Zn atoms in the substrate can be detected through the film. This interesting approach allows the coherent fraction of an element of a substrate below an interface to be probed *in situ*. For the Zn fluorescence, the coherent fraction is lower near the interface than in the bulk. These results should relate to strains and defects on both sides of the interface.

© 2004 International Union of Crystallography
Printed in Great Britain – all rights reserved

1. Introduction

X-ray standing waves constitute nowadays a well acknowledged technique for surface sciences [see for example the review by Zegenhagen (1993) for the earlier development of the XSW]. XSW generated on a crystal surface with a Bragg reflection have been extensively used to localize adatoms on the surface (Andersen *et al.*, 1976; Cowan *et al.*, 1980). One can find the same principle in the case of a mirror with grazing total reflection (Bedzyk *et al.*, 1990; Wang *et al.*, 1991) or in the case of a multilayer (Abruña *et al.*, 1990). From the first XSW works by Batterman (1964, 1969), the XSW have been used to probe atoms in a bulk crystal matrix (Golovchenko *et al.*, 1974; Materlik & Zegenhagen, 1984; Hertel *et al.*, 1985). In spite of all progress, the use of XSW in thin films has been very limited for several reasons. The XSW generated with a substrate reflection are not suitable for localizing atoms in a thin film because of the lattice mismatch between substrate and film. No structural information can be expected, except for the cases of a few monolayers of atoms (Koëbel *et al.*, 1997) or a thin film with a small mismatch with the substrate (Zegenhagen *et al.*, 1989). The use of the XSW generated by the substrate allows one to analyse the substrate quality under an ultrathin film (Zegenhagen *et al.*, 1990, 1995). Film reflections have been used for the cases where a kinematical approach is possible (Kazimirov *et al.*, 1997, 1998), *i.e.* the film thickness is small with respect to the extinction distance. In that case, the drawback of a weak XSW intensity (fluorescence modulation in % range) is compensated by the advantage of having a large angular range (fraction of a degree). In particular, this method was successfully applied to determine the polarity of ferroelectric thin films (Bedzyk *et al.*, 2000; Marasco *et al.*, 2001). For thin films of thickness a fraction of the extinction distance, the fundamental difficulty is the existence of two wavefields in a thin film, as is well known within the dynamical theory. This means that the total interference between the two transmitted beams and the two reflected ones gives rise to XSW continuously variable along the depth in the film. This variation of the XSW is *a priori* altering the structural information on the atomic positions in the film. This may be the basic reason why the XSW technique has not been developed in this case. One may notice a recent study of the XSW in multilayered crystal systems by Kohn (2002). To our knowledge, the only theoretical analysis has been given by Authier *et al.* (1989) for a thin film with a graded layer at the interface. In that case, the X-ray fields in the film were obtained by solving numerically the Takagi–Taupin equations. The authors pointed out that, even integrating over all the film, an XSW signal remains, *i.e.* the total X-ray intensity is different for two positions with respect to the film reflecting planes. Thus it

 DOI: 10.1107/S0108767304014473

Table 1
Parameters used for $00\bar{2}$ reflection at wavelengths of 1.25 and 1.35 Å in the case of $Zn_{0.94}Co_{0.06}O$ thin film of 0.67 µm thickness on $ZnO(00.\bar{1})$–O substrate.

		ZnO	$Zn_{0.94}Co_{0.06}O$
	Parameter of the c axis (Å)	5.207	5.224
For λ = 1.25 Å	Absorption coefficient (cm^{-1})	1099.0	1056.2
	Absorption coefficient of Zn $K\alpha$ (1.44 Å) fluorescence (cm^{-1})	212.6	260.8
	Extinction distance (µm)	2.27	2.31
	Structure-factor phase	0.128 π	0.128 π
	Darwin width of the reflection ($''$)	11.7	–
	FWHM of the film reflection ($''$)	–	21.9
For λ = 1.35 Å	Absorption coefficient (cm^{-1})	178.4	219.6
	Absorption coefficient of Co $K\alpha$ (1.79 Å) fluorescence (cm^{-1})	–	378.3
	Extinction distance (µm)	2.27	2.31
	Structure-factor phase	–	0.090 π
	Darwin width of the reflection ($''$)	12.7	–
	FWHM of the film reflection ($''$)	–	24.6

seems that the XSW in a thin film can be used to localize atoms, even if caution must be taken in this case in comparison with classical XSW on the bulk crystal surface.

Besides the atom localization, the so-called coherent fractions of the atoms probed are other interesting parameters provided by the XSW technique. If the significance of the coherent fraction is obvious for one monolayer of adatoms on a surface, its meaning becomes complicated when the XSW signal is integrated over a depth as in a thin film or the substrate. Because the XSW require a perfect coherence between the reflected and direct beams through the depth, defects can contribute to decrease the coherent fractions. The defects may be local like lattice distortions from atom substitutions, interstitial occupancies or vacancies. They can also be of long range such as dislocations, stacking faults, deformation and microstructure in thin films or crystal bending in a heterostructure. In thin films examined by Kazimirov *et al.* (1998), coherent fractions of about 0.36 were found and they are low in comparison with the case of surface XSW (above 0.9 for the case of one atomic site). Probably in order to distinguish the case of thin films from the classical ones, the term 'static Debye–Waller factor' instead of coherent fractions was used by the authors to specify the crystalline quality of the films. In fact, the difficulty in the case of thin films is to make the difference between the local structural disorder and the global crystalline quality of the film. For the present case of a $Zn_{1-x}Co_xO$ thin film, the question is to know whether the coherent fraction of Co atoms reflects the specific structural disorder of Co atoms or the general quality of the film. We make a comparison of Co atoms with the matrix elements of Zn atoms in the film. Furthermore, the coherent fraction of Zn atoms in the film is compared with that of Zn atoms in the substrate *in situ* and of Zn atoms in a reference substrate (without film).

In this paper, the case of a $Zn_{0.94}Co_{0.06}O$ epilayer on a $ZnO(00.\bar{1})$–O substrate will be analysed. $Zn_{1-x}M_xO$ (M is a magnetic transition metal) is, among the so-called diluted magnetic semiconductors (DMS), an interesting candidate as a room-temperature ferromagnetic material for spin electronics (Dietl *et al.*, 2000; Ueda *et al.*, 2001; Saeki *et al.*, 2001). The incorporation of magnetic atoms in the ZnO matrix can be up to 30%. The occupancy of magnetic atoms in either a substitutional Zn site or an interstitial one, or even their clustering, have a direct consequence on the magnetic behaviour of the film. Usually, the structural information on the incorporated atoms is deduced from indirect and global methods such as X-ray diffraction (Fukumura *et al.*, 1999). A direct method using the XSW seems to be very useful in this case for the information on both position and coherent fraction of incorporated atoms in the film. As indicated above, the structural order of the heterostructure is analysed with the Zn atoms. We will recall below basic characteristics of the XSW in a bulk crystal and extend the XSW to the case of a substrate under a thin film, *i.e.* the XSW generated by the substrate reflection for which the thin film can be considered as incoherent. Within the dynamical theory, we will detail the characteristics of the XSW generated across the main peak of a thin-film rocking curve.

2. Theory

The XSW features will be discussed using the $00\bar{2}$ reflection at two wavelengths (1.25 and 1.35 Å) just below and above the Zn K-absorption edge (Table 1). The wurtzite structure of ZnO (space group $P6_3mc$, a = 3.250 and c = 5.207 Å) is displayed in Fig. 1. The extinction distance Λ_r (real part of the complex extinction distance Λ) is about 2.27 µm at the two wavelengths, while the linear absorption coefficient μ increases dramatically from 178.4 cm^{-1} at 1.35 Å to 1099.0 cm^{-1} at 1.25 Å. The structure factors for the thin film $Zn_{0.94}Co_{0.06}O$ have been calculated (Soyer, 1995), taking into account the proportions of Zn and Co atoms. At 6% Co in the film, the diffraction parameters such as the extinction distance Λ_r and the linear absorption μ do not change significantly

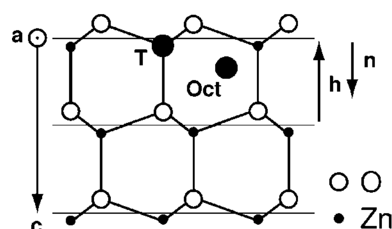

Figure 1
View of the ZnO structure along the a-axis direction. T is the tetrahedral substitutional site for Co atoms and Oct the octahedral interstitial site. Horizontal lines indicate the positions of the reflecting planes associated with the reflection $\mathbf{h} = 00\bar{2}$ and $\mathbf{n}$ is the normal vector used in the paper.

from the ZnO crystal. The only critical change concerns the c-axis parameter. For the $00\bar{2}$ reflection at 1.25 Å, the Bragg angle of the epilayer is about 166″ smaller than that of the substrate. Therefore, for the epilayer, the c-axis parameter is equal to 5.224 Å and the lattice mismatch is 0.3%. For the calculation, this value of c-axis parameter (5.224 Å) has been used for $Zn_{0.94}Co_{0.06}O$. The film thickness t used for the calculation is 0.67 µm, *i.e.* the ratio t/Λ_r is equal to 0.3. Principles of the treatments of the X-ray wavefields from the dynamical theory are given below for the cases of a bulk crystal, a substrate and a thin film. Further details for X-ray fields in a thin film can be found in Appendix *A*.

Only a symmetric reflection $\mathbf{h}$ is considered here with the dielectric displacement in σ polarization. The notations used are according to Authier (1986), except for the reflecting vector $\mathbf{h}$. The unit vector $\mathbf{n}$ normal to the crystal surface is directed into the crystal and $\mathbf{h}$ outwards. The complex incidence deviation parameter η is defined by $\eta = [(\theta - \theta_B)\sin 2\theta_B + \chi_o]/(\chi_h\chi_{\bar{h}})^{1/2}$, where θ_B is the Bragg angle and χ_o, χ_h and $\chi_{\bar{h}}$ are the Fourier components of the dielectric susceptibility. The extinction distance Λ is given by $\Lambda = \sin\theta_B/k(\chi_h\chi_{\bar{h}})^{1/2}$; k is the magnitude of the incident wavevector. The real part η_r of the incidence deviation parameter is directly related to the angular incidence.

2.1. XSW in a bulk crystal

In a bulk crystal, the fluorescence collected from any depth z is proportional to the local X-ray intensity and the absorption of the fluorescence photons inside the crystal:

$$\exp[-z/z'_o - z/z_o(\eta)]\{1 + R^{(B)}(\eta) + 2[R^{(B)}(\eta)]^{1/2}\cos[\Psi^{(B)}(\eta) - 2\pi\mathbf{h}\cdot\mathbf{r}]\}.$$

The intensity of the incident beam is put to 1 for the sake of simplicity. $R^{(B)}(\eta)$ is the reflectivity and $\Psi^{(B)}(\eta)$ the phase of the reflected beam relative to the incident one. $z_o(\eta)$ is the beam penetration depth and z'_o the fluorescence escape depth. It should be noticed that $z_o(\eta)$ is strongly dependent on the incidence across a Bragg reflection, while z'_o is only related to the fluorescence absorption coefficient μ' and the photon emergence angle δ: $z'_o = \sin\delta/\mu'$. The angle δ is referred to the photon path inside the crystal and it is slightly different from the one out of the crystal because of the refraction. The coherent fraction F_h and position P_h of fluorescent atoms are defined from a normalized atom distribution $\rho(\mathbf{r})$ within one lattice spacing:

$$F_h\exp(i2\pi P_h) = \int\rho(\mathbf{r})\exp(i2\pi\mathbf{h}\cdot\mathbf{r})\,\mathrm{d}^3\mathbf{r}.$$

Defining an effective depth $z_{o\,\mathrm{eff}}(\eta)$ equal to $z'_o z_o(\eta)/[z'_o + z_o(\eta)]$ and integrating over the crystal depth, one obtains the total fluorescence collected $Y^{(B)}(\eta)$ as follows:

$$Y^{(B)}(\eta) \propto z_{o\,\mathrm{eff}}(\eta)\{1 + R^{(B)}(\eta) + 2[R^{(B)}(\eta)]^{1/2} \times F_h\cos[\Psi^{(B)}(\eta) - 2\pi P_h]\}. \quad (1)$$

One remarks that the effective depth $z_{o\,\mathrm{eff}}(\eta)$ is always smaller than $z_o(\eta)$ or z'_o. Thus, in setting the detector at grazing angles (δ less than 1°), only the fluorescence of superficial layers of the crystal is collected, as was shown by Patel & Golovchenko (1983). For the present work, the emergence angle δ will be slightly varied in order to probe the Zn atoms as a function of the depth. One should notice that, from the depth $z_{o\,\mathrm{eff}}$, the fluorescence collected is smaller than the one from the surface by a factor of e^{-1}. When considering the crystal depth probed by the XSW, it is more suitable to take $2\times z_{o\,\mathrm{eff}}$. In such a way, the zone from the surface to a depth of $2z_{o\,\mathrm{eff}}$ contributes to 86% of the total fluorescence collected (instead of 63% for $z_{o\,\mathrm{eff}}$). In order to facilitate the relative comparison between different measurements through this paper, the crystal depth probed by the XSW will be defined as the depth from which the fluorescence collected is smaller than that at the surface by a factor of e^{-2}.

2.2. XSW in a substrate under an epilayer

Around a substrate Bragg reflection, the XSW are generated in a substrate under a thin film. For the film thickness considered here and when substrate and film reflections are well separated in angles, the film does not affect the X-ray beams except for absorption. However, one should pay attention to two points not treated here: (i) for close substrate and film reflections, a full dynamical treatment is necessary as shown in Appendix *A*; (ii) for thinner films, a coherent fluorescence signal comes also from the film (Zegenhagen *et al.*, 1989). For the present case, the reflectivity can be considered to be the same as for a bulk crystal with a constant absorption factor: $\exp[-2t/z_o^{(F)}]R^{(B)}(\eta)$, where t is the film thickness. The beam penetration depth $z_o^{(F)}$ in the thin film is related to the absorption coefficient $\mu^{(F)}$ and the substrate Bragg angle θ_B: $z_o^{(F)} = \sin\theta_B/\mu^{(F)}$. For the fluorescence from any depth z in the substrate ($z > t$), one should take into account the beam penetration through the thin film $\exp[-t/z_o^{(F)}]$ and in the substrate $\exp[-(z-t)/z_o(\eta)]$, as well as the fluorescence absorption in the substrate $\exp[-(z-t)/z'_o]$ and through the thin film $\exp[-t/z_o'^{(F)}]$. The fluorescence escape depth in the thin film $z_o'^{(F)}$ is related to the fluorescence absorption coefficient $\mu'^{(F)}$ and the emergence angle δ: $z_o'^{(F)} = \sin\delta/\mu'^{(F)}$. Thus the fluorescence from depth z is given by

$$\exp[-t/z_o'^{(F)} - t/z_o^{(F)} - (z-t)/z'_o - (z-t)/z_o(\eta)] \times \{1 + R^{(B)}(\eta) + 2[R^{(B)}(\eta)]^{1/2}F_h\cos[\Psi^{(B)}(\eta) - 2\pi P_h]\}.$$

The total fluorescence from the substrate is then obtained by integration over the substrate depth: $\exp[-t/z_o'^{(F)} - t/z_o^{(F)}]Y^{(B)}(\eta)$. The substrate depth probed by the XSW, defined with a reduction of e^{-2} for the fluorescence with respect to the surface, corresponds to the depth of $z_{o\,\mathrm{eff}}(\eta)[2 - t/z_o'^{(F)} - t/z_o^{(F)}]$.

Owing to the misfit between film and substrate, an incoherent fluorescence yield for Zn atoms is also excited in the film with the XSW generated by a substrate Bragg reflection. For any depth z in the thin film ($0 < z < t$), one should consider the absorption of the direct beam $\exp[-z/z_o^{(F)}]$, the one of the reflected beam $\exp[-t/z_o^{(F)} - (t-z)/z_o^{(F)}]$ and the fluorescence absorption $\exp[-z/z_o'^{(F)}]$. This means that the fluorescence from the depth z is proportional to $\exp[-z/z_o'^{(F)}]\times$

$\{\exp[-z/z_o^{(F)}] + \exp[-t/z_o^{(F)} - (t-z)/z_o^{(F)}]R^{(B)}(\eta)\}$. A scaling factor should be added with respect to the fluorescence from the substrate because of a lower density of Zn atoms in the thin film than in the substrate, *i.e.* fewer Zn atoms in the film composition and the unit cell is larger. After integration, the fluorescence from the whole thin film has the form $A + BR^{(B)}(\eta)$, where A and B are the proportional constants of the fluorescence excited by the direct and reflected beam, respectively.

The total fluorescence yield $Y^{(S)}(\eta)$ from the film and the substrate is

$$Y^{(S)}(\eta) \propto [A + BR^{(B)}(\eta)] + \exp[-t/z_o'^{(F)} - t/z_o^{(F)}]Y^{(B)}(\eta). \quad (2)$$

As a function of the incidence η, the fluorescence from the film has the same shape as the reflectivity $R^{(B)}(\eta)$ (plus a constant A). The shape of the fluorescence from the substrate is similar to that of a bulk crystal [equation (1)]. Thus, the form of the total fluorescence $Y^{(S)}(\eta)$ is highly sensitive to the emergence angle δ, which determines the contribution of the substrate.

2.3. XSW in a thin epitaxic film

While in a bulk crystal only one wavefield with the energy flux directed inwards is present, two wavefields are excited in a thin film (*cf.* Appendix *A*). Thus, the transmitted and reflected intensities in the film, as well as the interference term, are all depth-dependent:

$$I(z,\eta) = |D_o(z,\eta)|^2\{1 + |\xi(z,\eta)|^2 + 2|\xi(z,\eta)|\cos[\Psi(z,\eta) - 2\pi\mathbf{h}\cdot\mathbf{r}]\}. \quad (3)$$

Here all quantities are referred to the film, namely the incidence deviation η is defined with respect to the Bragg angle of the thin film. $D_o(z,\eta)$ represents the complex amplitude of the transmitted beams, $\xi(z,\eta) = D_h(z,\eta)/D_o(z,\eta)$ is the amplitude ratio between the reflected and transmitted beams and $\Psi(z,\eta)$ the phase of $\xi(z,\eta)$. At Bragg reflection ($\eta_r \sim 0$, where η_r is the real part of η), the transmitted intensity $|D_o(z,\eta)|^2$ in the film exponentially decreases with $\Lambda_r/2\pi$ as the decay distance. Out of the main peak of the film rocking curve ($|\eta_r| > 3.5$ for the present case), the transmitted intensity $|D_o(z,\eta)|^2$ decreases slowly under the linear absorption effect and oscillates weakly with a period equal to the effective extinction distance $[\sim \Lambda_r/(\eta_r^2 - 1)^{1/2}]$.

The important quantities for the XSW are the ratio $|\xi(z,\eta)|$ and the phase $\Psi(z,\eta)$ between the reflected and transmitted beams. More precisely, the phase term concerns the difference $\Psi(z,\eta) - \varphi_h$ between $\Psi(z,\eta)$ and the structure-factor phase φ_h. In such a way, when $\Psi(z,\eta) - \varphi_h$ is equal to zero, the XSW antinode is on the reflecting planes and, when $\Psi(z,\eta) - \varphi_h$ is equal to π, the XSW antinode is at the middle between the reflecting planes. Fig. 2 displays the variation of $|\xi|$ and $\Psi - \varphi_h$ as a function of the incidence η_r on the surface, at the middle of the film and at the interface. $|\xi|$ on the surface shows the oscillations associated with a thin film as can be observed in the reflectivity ($R = |\xi|^2$ for $z/t = 0$). The amplitude of the oscillations decreases in the depth of the film ($z/t = 0.5$) and the period increases. Whatever the detailed interface structure, the boundary condition implies that the ratio $|\xi|$ is equal to the one of the substrate $|\xi^{(s)}|$ at the interface ($z/t = 1$), *i.e.* near zero. The substrate influence depends on the angular distance between the reflections of the substrate and the film and affects mainly the phase term (Fig. 2*b*). On the surface ($z/t = 0$), the phase $\Psi - \varphi_h$ oscillates around π at lower incidences ($\eta_r < -3.5$) and decreases to around 0 across the main peak of the film rocking curve. This means that the XSW antinode is around the middle between the reflecting planes at lower angles and moves around the reflecting planes across the main peak of the rocking curve. The situation is more complicated at higher angles close to the substrate reflection. The phase $\Psi - \varphi_h$ oscillates around 0 with increasing incidences ($3.5 < \eta_r < 10$ at $z/t = 0$). When the substrate influence is predominant ($\eta_r > 10$ at $z/t = 0$), the phase $\Psi - \varphi_h$ decreases continuously. The interface ($z/t = 1$) constitutes the other extreme case where only the substrate is important: $\Psi(z,\eta) = \Psi^{(s)}(\eta)$ for $z/t = 1$. For the present case, as the film reflection is at a lower angle than for the substrate, $\Psi - \varphi_h$ is equal to π at the interface. The important feature from the present analysis concerns the evaluation of the substrate influence on the XSW in thin films. When the substrate influence is low, *i.e.* for a film reflection at large angular distance from the substrate and for the upper part of the thin film, the XSW antinode oscillates around the middle between the reflecting planes at lower angles, moves to the reflecting planes across the main peak of the film reflection and oscillates around the reflecting planes at higher angles. In this case, the behaviour of XSW in the film is similar to that in a bulk

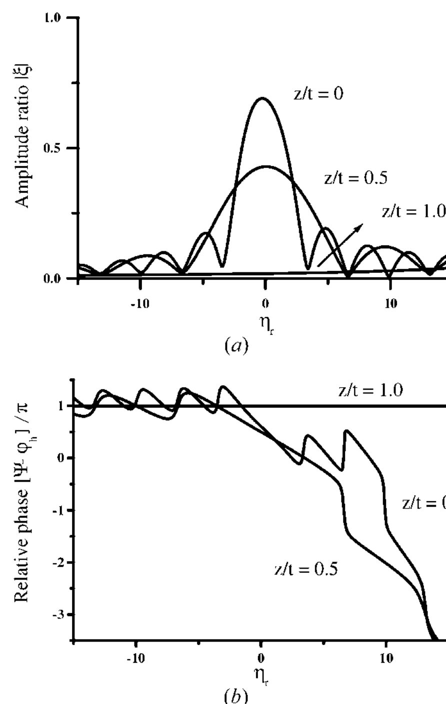

Figure 2
(*a*) Amplitude ratio $|\xi|$ and (*b*) relative phase $\Psi - \varphi_h$ as a function of the incidence η_r for a $Zn_{0.94}Co_{0.06}O$ film of 0.67 µm at λ = 1.25 Å, on the surface ($z/t = 0$), at the middle of the film ($z/t = 0.5$) and at the interface ($z/t = 1$).

crystal, except for the oscillations due to the existence of a second wavefield. When the substrate is predominant, *i.e.* for close film and substrate reflections or at a depth in the film, the XSW antinode continuously shifts with respect to the film reflecting planes, as a function of the incidences η_r.

Around the film reflection, the variation along the film depth z for the amplitudes and phases of the wavefields are related to the extinction distance Λ_r and the film thickness t, which are large in comparison with one lattice distance. These variations can be neglected within one lattice distance, so that a usual XSW treatment can be done locally in defining the coherent fraction F_h and position P_h from a normalized distribution $\rho(\mathbf{r})$ of fluorescent atoms. The local XSW intensity, *i.e.* the local dielectric displacement intensity, on a distribution $\rho(\mathbf{r})$ of atoms is then deduced from relationship (3) as

$$I_{\rm XSW}(z,\eta) = |D_o(z,\eta)|^2\{1+|\xi(z,\eta)|^2 + 2|\xi(z,\eta)|F_h\cos[\Psi(z,\eta)-2\pi P_h]\}. \quad (4)$$

The excited fluorescence $Y(\eta)$ is obtained by the integration over the film: $Y(\eta) \propto \int_0^t I_{\rm XSW}(z,\eta)\,{\rm d}z$. The fluorescence yield $Y(\eta)$ can be written in a form similar to the usual XSW in a bulk crystal:

$$Y(\eta) = Y_o(\eta) + Y_h(\eta) + 2Y_i(\eta)F_h\cos[\Psi_i(\eta)-2\pi P_h]. \quad (5)$$

$Y_o(\eta)$ and $Y_h(\eta)$ correspond to the background fluorescence excited respectively by the direct and reflected beams and do not contain any structural information on the fluorescent atoms. The third term, the interference one, is quantified by the amplitude $Y_i(\eta)$ and the phase $\Psi_i(\eta)$: $Y_i(\eta)\exp[i\Psi_i(\eta)] \propto \int_0^t |D_o(z,\eta)|^2\xi(z,\eta)\,{\rm d}z$.

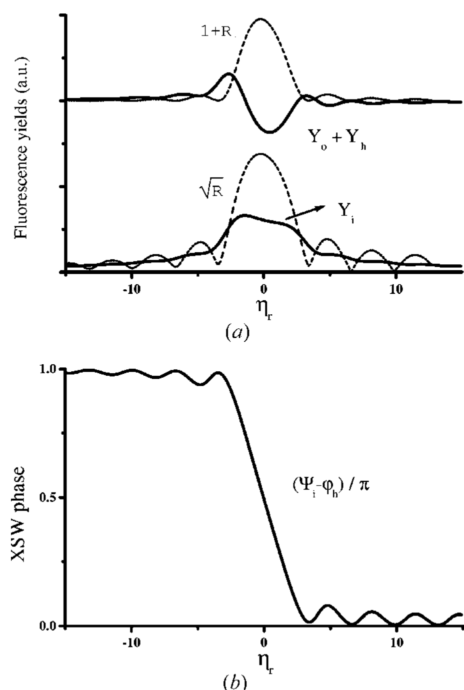

Figure 3
Integrated fluorescence yields and phase as a function of the incidence η_r for the $Zn_{0.94}Co_{0.06}O$ film at λ = 1.25 Å. (*a*) Background $Y_o + Y_h$ and interference Y_i fluorescences, compared with the corresponding surface XSW terms $1 + R$ and $R^{1/2}$. (*b*) XSW phase ($\Psi_i - \varphi_h$) with respect to the reflecting planes.

Fig. 3 displays the background fluorescence ($Y_o + Y_h$), the interference fluorescence amplitude (Y_i) and the phase $\Psi_i - \varphi_h$ as a function of the incidence (η_r). The background fluorescence ($Y_o + Y_h$) decreases during the film reflection owing to the reduction of the beam penetration depth under a Bragg reflection. The interference fluorescence only has a significant amplitude across the main peak of the rocking curve. This means that only the region around the main peak of a film rocking curve provides structural information on fluorescent atoms: secondary peaks come from the interference of the two wavefields inside the film and do not contain any information within one lattice distance. One should notice that the dynamical XSW signal of thin films is quite different from the XSW on the thin film surface or for thin films with the kinematical treatment: the background fluorescence $Y_o + Y_h$ is not proportional to $1 + R$ nor is the interference fluorescence Y_i proportional to $R^{1/2}$ (dashed lines in Fig. 3*a*). If the XSW signal contrast is defined as $2Y_i/(Y_o + Y_h)$, a maximal contrast of about 73% is found for the present case, in comparison with the maximal value of about 100% for the XSW on the bulk crystal surface. This order of contrast is general for films of thickness in the range of a fraction of the extinction distance and appears to be very suitable for the use of XSW as a probe.

The most important parameter is the phase $\Psi_i - \varphi_h$, in other words, the XSW antinode position with respect to the reflecting planes, averaged over the whole film. One can notice in Fig. 3(*b*) that, besides the oscillations typical of a thin film, the XSW phase has exactly the same evolution in comparison with the usual XSW, *i.e.* the XSW antinode moves from the middle between the reflecting planes to the reflecting planes when the main peak of the reflection is scanned from lower to higher angles. This result may be surprising because the local XSW in the depth of the film have continuous variations, especially for the angular region close to the substrate reflection (Fig. 2*b*). In fact, the lower part of the thin film has only a small contribution to the global XSW signal: as $|\xi|$ falls to near zero at the interface, the fluorescence from the lower part of the film contributes very weakly to the interference term, but essentially to the background excited by the direct beam.

A simulation of the total fluorescence yield $Y(\eta)$ for different values of the coherent position P is shown in Fig. 4. Different shapes of the fluorescence yield demonstrate a good sensitivity of the XSW method to determine the atom position in a film. In order to evaluate the experimental precision of the coherent position in a film in comparison with the case of the XSW on the bulk crystal surface, one should take into account the intrinsic XSW characteristics – a lower contrast, small phase oscillations and averaging over the film – and expected extrinsic factors, especially a lower crystalline quality for a film. Thus, it can be estimated that a precision of under 0.05 can be reached for the value of the coherent position, and this is to be compared with 0.01 for the XSW on the bulk crystal

surface. Such sensitivity is very suitable to solve a number of structural problems in a film, such as the atomic site determination. For the present case of $Zn_{1-x}Co_xO$, the distance between the tetrahedral substitutional and octahedral interstitial sites (Fig. 1) implies a difference of 0.27 in coherent positions for the $00\bar{2}$ reflection.

Around the film reflection, the fluorescence from the substrate constitutes an incoherent signal for Zn atoms. In order to collect only the contribution from the thin film, the detection angle δ is limited to a fraction of a degree. The photon escape depth $z_o'^{(F)}$ in the thin film can be reduced to smaller than the film thickness for the present case. Including the photon escape depth, the fluorescence yield given in (5) should be reformulated as $Y(\eta) \propto \int_0^t I_{\rm XSW}(z,\eta)\exp[-z/z_o'^{(F)}]\,{\rm d}z$.

3. Experiment

Thin epitaxic layers of $Zn_{1-x}Co_xO$ were grown on the $(00.\bar{1})$–O face of a ZnO crystal by pulsed laser deposition. The alternative growth was performed under a vacuum of 10^{-9} bar with targets of ZnO and CoO. An excimer KrF laser (λ = 248 nm, τ = 20 ns) was used at a fluence of 3×10^4 J m^{-2} and a repetition frequency of 2 Hz. The substrate–target distance was 5 cm and the substrate temperature about 823 K. Structural aspects of these films will be reported elsewhere (Zheng *et al.*, 2004). For the present study, the key point is to know whether the Co atoms are diluted in a ZnO matrix or if they are in the form of clusters. Results from diffraction techniques seem to indicate that the Co atoms are well diluted. No change in RHEED patterns was observed on a thin film and on the initial substrate surface. X-ray diffraction indicated that the *c*-axis parameter in $Zn_{1-x}Co_xO$ films linearly increases with the content of Co atoms. One should also mention that an EPR (electron paramagnetic resonance) study on a $Zn_{0.90}Co_{0.10}O$ film grown with the same conditions indicated that Co atoms are well distributed in the ZnO matrix (Jedrecy *et al.*, 2004). For the present case, a thin film of $Zn_{0.94}Co_{0.06}O$ of 0.67 µm thickness was chosen to carry out the XSW experiments, as well as a reference substrate from the same initial crystal block.

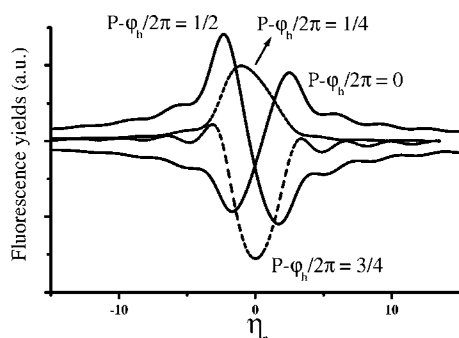

Figure 4
Total fluorescence yields as a function of the incidence η_r for the $Zn_{0.94}Co_{0.06}O$ film at λ = 1.25 Å, for different coherent positions: $P - \varphi_h/2\pi$ = 0, 0.25, 0.5 and 0.75.

XSW experiments were carried out at beamline D25B of the DCI storage ring (LURE, Orsay, France). The reflectivity was recorded with an NaI scintillator and the fluorescence with an Si(Li) solid-state detector. The monochromator was a four-reflection Si 111 channel-cut with an angular divergence of about 1″ (Boulliard *et al.*, 1992). Owing to the lattice mismatch between the monochromator ($d_{111\ \rm Si}$ = 3.1 Å) and the sample ($d_{00.2\ \rm ZnO}$ = 2.6 Å), the effective divergence due to the slightly dispersive geometry is estimated to be under 8″. For XSW profiles, the samples were rotated by a piezoelectric head with a relative precision of 0.01″. For Zn atoms, the wavelength of 1.25 Å just below the *K*-absorption edge was selected to get a high signal of Zn $K\alpha$ fluorescence. In probing Zn atoms in the substrate with the substrate reflection, a slit parallel to the sample surface was put on the detector aperture to ensure an equal emergence angle for photons collected and the detector was positioned at grazing angles. With the film reflection, the detection angle δ is limited to a fraction of a degree in order to collect only the contribution from the thin film. It is worth noticing that the photon escape depth $z_o'^{(F)}$ in the thin film is reduced from 38 µm with a normal emergence detection to 0.27 µm with a detection under 0.4°, *i.e.* an escape depth smaller than the film thickness. For Co atoms, the wavelength of 1.35 Å just above the Zn *K*-absorption edge was selected in order to eliminate the huge counting of Zn $K\alpha$ fluorescence and increase the counting efficiency for Co $K\alpha$. Furthermore, the detector was set at higher angles, above 10°, with the fully opened aperture.

4. Results and discussion

4.1. XSW in a ZnO$(00.\bar{1})$–O reference substrate

Prior to the study of the heterostructure, a measurement of the Zn-atom coherent fraction in a reference substrate was made. The obtained value will be used later as a standard. Substrates were obtained from hydrothermal ZnO crystal blocks of 1 cm^3 size. (00.1) slices of 0.35 mm thickness and 1 cm^2 size were mechanochemically polished with a roughness of less than 2 nm. Major crystal defects revealed by X-ray topography concern dislocations existing in the prismatic planes of {10.0} type (Zheng *et al.*, 2004). In order to avoid a possible evolution of the substrates during the growth process, the reference substrate was heated at 823 K under vacuum for 5 h, similar to the case of other substrates during the film growth. No change in extended crystal defects was seen in X-ray topography. The X-ray rocking curve with $00\bar{2}$ at the wavelength of 1.25 Å (reflectivity in Fig. 5) has a FWHM of 12.8″. This width fits well with the intrinsic reflection width and the instrumental divergence of about 5″. It indicates a high crystalline quality of the substrates.

For the Zn $K\alpha$ fluorescence detection, a slit of 0.4 mm height and parallel to the crystal surface limited the detector aperture. The detector was set about 4 cm away from the sample. This means that the detection angle δ was defined in general within ±0.3°. In fact, a relative accuracy of about ±0.1° can be reached for grazing emergence angles (δ < 1°).

As the fluorescence counting increases with the detection angle, most photons were collected from the upper part of the slit. The situation becomes special for δ close to zero: only one part of the slit above the crystal surface contributes to the detection. Zn $K\alpha$ fluorescence yields obtained at four detection angles are shown in Fig. 5. As expected in a bulk ZnO crystal (Fig. 1), the coherent position $P_{00\bar{2}}$ of Zn atoms deduced from Zn $K\alpha$ fluorescence yields is equal to zero. The value of $P_{00\bar{2}}$ of Zn atoms will be kept at zero for all the calculated curves below and excluded from the fitting parameters. It is worth noticing that $00\bar{2}$ and 002 reflections provide different XSW profiles. The coherent positions of Zn atoms measured here ascertained the expected polar face ZnO(00.$\bar{1}$) for the substrate (Bedzyk *et al.*, 2000).

The coherent fraction $F_{00\bar{2}}$ of Zn atoms was found to be 0.92 ± 0.04. The crystal depths probed by the XSW for the detection angles used are illustrated in Fig. 6. Out of the reflection range, the XSW probing depth is from 0.5 to 2.1 µm and it is essentially limited by the photon escape depth. Under the Bragg reflection, it is limited by both beam penetration depth and photon escape depth. For δ from 0.3 to 1.5°, the minimal value for the XSW probing depth is from 0.3 to 0.6 µm. This means that the structural order of Zn atoms is homogeneous until a depth of about 1 µm. The value of $F_{00\bar{2}}$ should be understood in considering the thermal Debye–Waller factor and the presence of crystal defects. The thermal agitation at room temperature (Albertsson *et al.*, 1989) leads to an ideal value of 0.97 for the coherent factor $F_{00\bar{2}}$. Thus a difference of 0.05 remains between the experimental value of 0.92 and the expected one of 0.97 for a perfect crystal. This difference is very small when one takes into account numbers of crystal defects present in oxide crystals, such as dislocations and oxygen vacancies. Strains of long range due to the crystal bending were also searched for by measuring the deviation in Bragg angle along the sample surface. No bending of the substrate was found within the experimental precision.

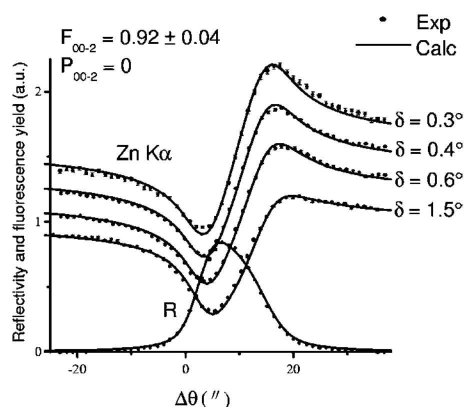

Figure 5
Experimental and calculated reflectivity R and normalized Zn $K\alpha$ fluorescence yields of a ZnO(00.$\bar{1}$)–O reference substrate (without film) using the $00\bar{2}$ reflection at λ = 1.25 Å, with different detection angles δ. The fluorescence yields out of the Bragg reflection are normalized to unity. For visibility, successive vertical shifts of 0.2 are made on the curves for δ = 0.6, 0.4 and 0.3°.

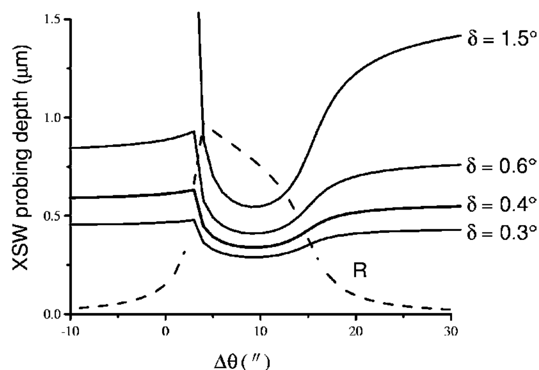

Figure 6
Estimated crystal depths probed by the XSW in a ZnO(00.$\bar{1}$)–O bulk crystal under $00\bar{2}$ reflection at λ = 1.25 Å, with different detection angles δ. The theoretical reflectivity R (dashed line) is inserted for the angular scale.

4.2. XSW in a $Zn_{0.94}Co_{0.06}O$ epilayer on ZnO(00.$\bar{1}$)–O substrate

Similar angular measurements on the heterostructure revealed an epitaxy-induced bending with a curvature radius of 20 ± 1 m. The bending induces an angular variation of about 100″ over the whole sample surface (1 cm), *i.e.* about eight times larger than the substrate reflection width. In order to minimize the bending effect on the XSW, the incident beam was limited by a slit of about 45 µm height (and 2 mm width). This implies an irradiated surface on the sample of about 187 µm height. The angular variation within the irradiated surface is reduced to 1.9″ and becomes negligible with respect to the reflection widths.

From the reflectivities (Fig. 7) of the $Zn_{0.94}Co_{0.06}O$ film on ZnO(00.$\bar{1}$)–O, the differences in Bragg angles between the film and substrate were found to be 165.6″ at λ = 1.25 Å and 180.2″ at λ = 1.35 Å. The averaged c-axis parameter in the film is deduced as 5.224 ± 0.002 Å, *i.e.* a lattice mismatch of 0.3% with the substrate. Across the Zn K-absorption edge, the reflectivity of the substrate reflection falls from 0.85 at λ = 1.35 Å to 0.46 at λ = 1.25 Å. The reduction of the reflectivity in comparison with the reference substrate (0.84 at λ = 1.25 Å)

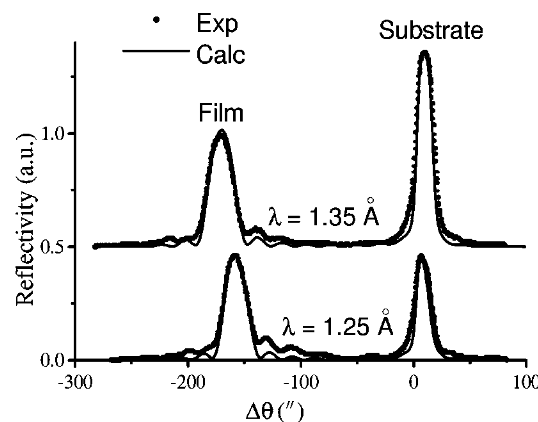

Figure 7
Experimental and calculated reflectivity of the heterostructure, with $00\bar{2}$ reflection at λ = 1.25 and λ = 1.35 Å. The baseline of the curves at 1.35 Å is vertically shifted for visibility.

corresponds to the absorption by a film of 0.67 μm thickness. This was confirmed by the oscillations in the rocking curves, which provided an evaluation of 0.67 ± 0.03 μm for the film thickness.

Sharp peaks were observed for both film and substrate reflections. The peak widths at λ = 1.25 Å, 23.5 and 17.0″, respectively, for the film and the substrate, agree with the intrinsic ones and an instrumental divergence of 5″. To our knowledge, this is the highest crystalline quality observed until today in ZnO thin films. However, differences in the peak shapes exist between the experimental and calculated reflectivities. One recognizes a broad component beyond both thin film and substrate peaks. This could come from elastic and inelastic scattering processes, since the broad component seems to increase below the Zn *K*-absorption edge at λ = 1.25 Å. Another possibility concerns strains around the film–substrate interface. Indeed, interface models were proposed by several authors including a graded layer at the interface in order to get a smooth elastic transition between film and substrate (Bensoussan *et al.*, 1987). It was claimed that such a graded layer improved the agreement between the experimental and calculated reflectivities. In the frame of this work, a better fitting of the reflectivities will not be investigated. It does not seem possible to propose a realistic and general strain model, including all the necessary ingredients: presence of dislocations, epitaxy-induced bending, stress relaxation at the interface, oxygen vacancies and insertion of Co atoms.

4.2.1. Location of Co atoms. For Co atoms diluted in a ZnO matrix, both atomic site and order are important information for the knowledge of a diluted magnetic semiconductor. The wavelength of 1.35 Å, above the Zn *K*-absorption edge, was selected in order to reduce the inelastic scattering in the heterostructure and increase the Co *Kα* fluorescence counting. As Co atoms are only present in the thin film, a usual detection was used with a fully opened detector aperture and at high angles (from 10 to 30°). It was checked that the shape of the Co *Kα* fluorescence yields did not depend on the detection angle. The XSW parameters obtained from the experiments for Co atoms (Fig. 8) are: a coherent position, $P_{00\bar{2}} = 0.00 \pm 0.03$, which corresponds to the position of Zn atoms in ZnO, and a coherent fraction, $F_{00\bar{2}} = 0.57 \pm 0.05$. The value of the coherent position suggests that Co atoms are at the tetrahedral substitutional site, but the low value of the coherent fraction troubled this direct interpretation from the coherent position to the atomic position. For Zn atoms, there is only one atomic site in the ZnO crystal structure. In principle, this is not the case for inserted Co atoms, which could be at either the octahedral site or the tetrahedral one (Fig. 1). If a model of the two atomic sites is used for Co atoms in order to fit with the measured coherent fraction of 0.57, no solution can be found. Even with 50% of Co atoms on octahedral sites which are located at −0.265 with respect to the lattice spacing $d_{00\bar{2}}$, the coherent fraction $F_{00\bar{2}}$ found is 0.67 and it is the lowest value: $0.5\exp(i2\pi 0) + 0.5\exp(-i2\pi 0.265) = 0.67\exp(-i2\pi 0.133)$. In such a case, the resulting coherent position, $P_{00\bar{2}} = -0.133$, is centred between the two atomic sites and it is too different from the experimental value. A two-site model for Co atoms cannot explain the reduction of the coherent fraction. To explain the low value of the coherent fraction, there are two possibilities. (i) A clustering of a fraction of the inserted Co atoms. It should be noted that, if ferromagnetism has been detected in $Zn_{1-x}Co_xO$ films (Ueda *et al.*, 2001) and in $Zn_{1-x}V_xO$ films (Saeki *et al.*, 2001), its origin is not really understood. Moreover, the ferromagnetism evidenced in Co-doped TiO_2 has been, in some cases, attributed to Co atoms clustering (Kim *et al.*, 2003; Chambers *et al.*, 2003). (ii) An important density of crystalline defects in the epilayer. In this case, the notion of static Debye–Waller factor is often used. The choice between the two possibilities can be made by measuring the coherent fraction of Zn atoms in the film.

4.2.2. Zn atom coherent fraction. Zn atoms in the film may give information complementary to that obtained with Co atoms. The fluorescence contribution of the substrate can be eliminated at small grazing emergence. For the XSW profile shown in Fig. 9, the detection angle used was about 0.4°. At

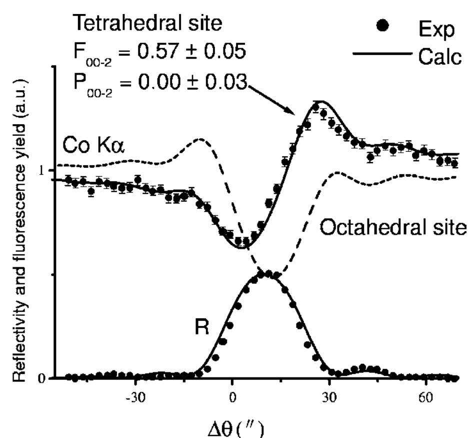

Figure 8
Experimental and calculated reflectivity *R* and normalized Co *Kα* fluorescence yield of the $Zn_{0.94}Co_{0.06}O$ film, using $00\bar{2}$ film reflection at λ = 1.35 Å and with a fully opened detector aperture. The dashed curve represents the simulation of Co *Kα* fluorescence yield for Co atoms at octahedral interstitial sites.

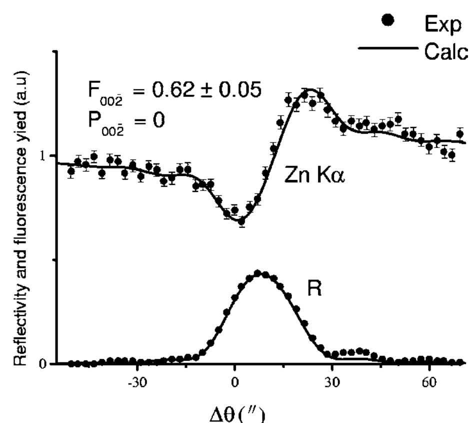

Figure 9
Experimental and calculated reflectivity *R* and normalized Zn *Kα* fluorescence yield of the $Zn_{0.94}Co_{0.06}O$ film, using $00\bar{2}$ thin film reflection at λ = 1.25 Å and with a grazing emergence angle of ≃0.4°.

this detection angle and around the film reflection, the film depths probed by the XSW range from 0.14 to 0.54 μm. Thus, the XSW signal comes from almost the whole film thickness. The coherent fractions $F_{00\bar{2}}$ for Zn atoms in the thin film was found to be 0.62 ± 0.05. Therefore, for Co and Zn atoms, the coherent fraction is roughly the same. So the clustering is not at the origin of the low value for the Co atom coherent fraction. Moreover, the discrepancy between the values for Zn atoms in the epilayer and in the reference substrate is rather surprising if the sharpness of the rocking curves is taken into account. To understand this, a study of Zn atom coherent fraction in the substrate, under the film, has been made.

4.3. XSW in the substrate under the thin film

In order to probe Zn atoms in the substrate under the thin film, detection angles slightly larger than in the case of the reference substrate were used (Fig. 10). With increasing angles from 0.9 to 6.0°, the shapes of Zn $K\alpha$ fluorescence yields vary as expected from the relationship (2). At low angles (0.9 and 1.0°), the incoherent signal from the thin film is predominant. The fluorescence yields have a shape similar to that of the reflectivity and the remaining difference comes from the signal of the substrate. At higher angles, the XSW signal from the substrate was increased by the increasing photon escape depth. In excluding the film thickness, the substrate depths probed by the XSW were estimated (Fig. 11). Under the substrate Bragg reflection, the minimal depths probed by the XSW range from 0.14 to 0.50 μm, of the same order as for the reference substrate. Outside the substrate rocking curve, the XSW probing depths from 0.4 to 4.8 μm were higher with the angles used higher than for the reference substrate.

The surprising results concern the coherent fractions $F_{00\bar{2}}$, which are not homogeneous as a function of the substrate depth (Table 2), in apparent contradiction with the measurements made in the reference substrate. The value of $F_{00\bar{2}}$ is about 0.60 close to the interface, when Zn atoms were probed for depths from 0.14 to 0.40 μm with the detection angle at 0.9°. A value of $F_{00\bar{2}}$ of about 0.90, close to the one in the reference substrate, was found at high angles, when depths from 0.5 to 4.8 μm were probed. The precision of the XSW measurements at grazing angles is lower (±0.10) than at higher angles (±0.05) because of a lower counting efficiency and a lower XSW signal from the substrate. In spite of this, the variation of $F_{00\bar{2}}$ for Zn atoms from the interface to the substrate depth was well established within the experimental errors. A coherent fraction of 0.60 is quite low and it cannot be understood in terms of local structural disorder for Zn atoms. With regard to the high crystalline quality of the substrates and the measurements in the reference substrate, Zn atoms should be located at the expected unique site inside the unit cell. Thus, the reduction of the coherent fractions near the interface should come from a structural disorder of long range, induced by the epitaxy and probably also by defects. Epitaxy-induced strains in thin films have been widely investigated, but there are very few studies on the influence of the epitaxy on the substrate. Thus, the XSW experimental data obtained here provide new and interesting indications on the strains in a substrate in the vicinity of the interface.

Table 2
Coherent fractions of Zn atoms using $00\bar{2}$ reflection at λ = 1.25 Å in a ZnO(00.$\bar{1}$)–O reference substrate and in the heterostructure.

	Detection angle δ (°)	Coherent fraction $F_{00\bar{2}}$	Estimated range of XSW probing depth (μm)
Zn atoms in the ZnO(00.$\bar{1}$)–O reference substrate	0.3	0.92 ± 0.04	0.29–0.48
	0.4		0.34–0.63
	0.6		0.41–0.93
	1.5		0.55–2.14
Zn atoms in $Zn_{0.94}Co_{0.06}O$ thin film	0.4	0.62 ± 0.05	0.14–0.54
Zn atoms in the ZnO(00.$\bar{1}$)–O substrate under the thin film	0.9	0.60 ± 0.10	0.14–0.40
	1.0	0.75 ± 0.08	0.17–0.53
	2.5	0.85 ± 0.05	0.39–2.14
	3.0	0.85 ± 0.05	0.42–2.60
	4.5	0.90 ± 0.05	0.47–3.78
	6.0	0.90 ± 0.05	0.50–4.75

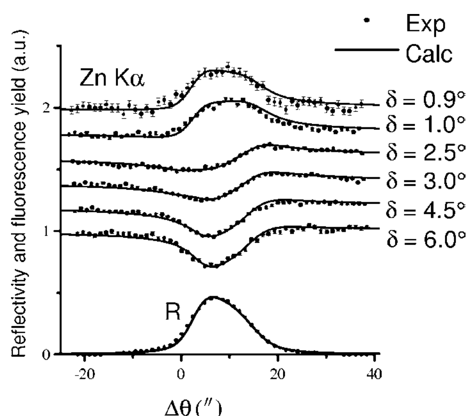

Figure 10
Experimental and calculated reflectivity R and normalized Zn $K\alpha$ fluorescence yields from the substrate under the film, using $00\bar{2}$ substrate reflection at λ = 1.25 Å and with different detection angles δ. The fluorescence yields out of the Bragg reflection are normalized to unity. For visibility, successive vertical shifts of 0.2 are made for the upper fluorescence curves.

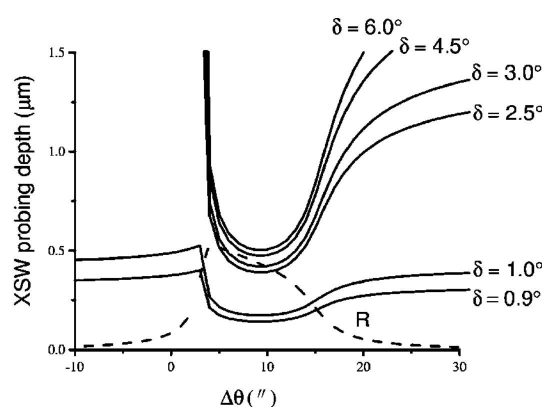

Figure 11
Estimated ZnO(00.$\bar{1}$)–O substrate depths probed by XSW under the $Zn_{0.94}Co_{0.06}O$ film, using $00\bar{2}$ substrate reflection at λ = 1.25 Å. The theoretical reflectivity R (dashed line) is inserted for the angular scale.

4.4. Discussion

The main results extracted from the XSW experiments are: (i) Co atoms are located at Zn sites; (ii) their coherent fraction is rather low but Zn atoms in the film have roughly the same coherent fraction; (iii) under the interface, in a range of 1 µm, Zn atoms of the substrate retain this low value. On the other hand, when probing a greater depth, the value measured in the reference substrate is found again. Owing to (iii), the rather low values of Co and Zn atom coherent fractions in the epilayer cannot be explained by an atomic structural disorder. These should be related to the effect on the XSW of the strains always present in a heterostructure.

A film grown on a thick substrate induces stresses in the heterostructure. Their study has given rise to a very large amount of publications, especially for lattice-mismatched semiconductors. Two main relaxation stages are usually considered. (i) Elastic relaxation stage. The growth of a pseudomorphic layer onto a substrate allows the elastic accommodation of the lattice misfit by matching lattice parameters at the interface. The stresses stored in the epilayer induce a curvature of the substrate. (ii) Plastic relaxation stage. Above the so-called critical thickness, whose value depends on the lattice mismatch, misfit dislocations appear at the interface.

For more than 30 years, X-ray diffraction has been used to characterize heterostructures. In the case of the elastic relaxation, it allows one to obtain the radius of curvature of the substrate and average stresses in the thin film (Rozgonyi & Ciesielka, 1973; Estop *et al.*, 1976; Henein & Wagner, 1983). But 'classical' diffraction is inadequate to reveal what many authors have observed by different means: the strain near the surface of an epilayer is low and increases as the depth increases. This fact, valid for epilayers with a thickness below or above the critical one, has been evidenced by Raman scattering and Rutherford backscattering spectroscopy (RBS) (Olego *et al.*, 1987; Lovergine *et al.*, 1995).

Therefore, our results concerning the Zn atoms can be interpreted as follows. (i) The epilayer (0.67 µm) is not thick enough to allow a depth profiling of elastic strains *via* the measurement of the coherent fraction. So their low value should be related to an average value of the strains in the film. (ii) In the substrate, the increase of the coherent fraction with the depth probed by XSW reveals the strain gradient. By using an appropriate model of the strain gradient on both sides of the interface, the correlation between the coherent fraction and the strain field could be obtained. To our knowledge, only one theoretical paper has been published on this subject (Kato, 1998). It concerns a distorted layer inserted in a thick crystal and shows that XSW are more sensitive to any lattice distortion than the rocking curve.

5. Conclusions

The dynamical treatment indicates that XSW, generated around the main peak of a thin epilayer rocking curve, have the same form as XSW on a bulk crystal surface. The XSW phase $\Psi_i - \varphi_h$ keeps the fundamental characteristic: it moves from around π to around 0 across the main peak of a film reflection. This means that, in averaging over all the film, the apparent XSW antinode moves into the sample from a position between the reflecting planes to a position around the reflecting planes when the sample is turned from lower to higher angles. It is worth noticing that the interface layer essentially contributes to the background fluorescence, while the upper part of the film contributes to the XSW signal. The last point can be enhanced by a grazing detection of the fluorescence. The use of the XSW generated by a substrate reflection proposed here is an interesting approach to probe a substrate *in situ* under a film. Combined with a grazing detection, a depth profiling of the crystalline perfection becomes possible in the substrate. However, studies are still needed to associate the measured coherent fractions with the defects and strains in a heterostructure. The effects of the defects on the X-ray coherence should be also detailed.

In the $Zn_{0.94}Co_{0.06}O$ film, Co atoms were found to be at the substitutional Zn site with a coherent fraction of about 0.57. Comparing with the host Zn atoms in the thin film for which a similar coherent fraction was found, we believe that the low coherent fraction is not related to a specific Co-atom disorder but to strains present in the film. Their origin is probably related to the defects involved in the stress relaxation at the interface. An important fact is that their effects extend over the substrate depth in the µm range. The first results obtained allow further investigations of the strains in alloy films, in particular in diluted magnetic semiconductors. For the last class of materials ($Zn_{1-x}M_xO$ with M = Co, V, Mn, ...), the structural information as a function of the type and amount of the transition metal and as a function of other characteristics of the film (oxygen content, charge carriers *etc.*) is important for the understanding of the magnetic correlation and behaviour in these films.

APPENDIX *A*
XSW in a thin epitaxic film

The non-zero component of the dielectric displacement D in σ polarization can be written in the form

in vacuum ($z<0$)
$$D = D_o^{(a)} \exp(-i2\pi \mathbf{K}_o^{(a)} \cdot \mathbf{r}) + D_h^{(a)} \exp(-i2\pi \mathbf{K}_h^{(a)} \cdot \mathbf{r})$$

in the film ($0<z<t$)
$$D = D_o^{(1)} \exp(-i2\pi \mathbf{K}_o^{(1)} \cdot \mathbf{r}) \times [1 + \xi^{(1)} \exp(-i2\pi \mathbf{h} \cdot \mathbf{r})] + D_o^{(2)} \exp(-i2\pi \mathbf{K}_o^{(2)} \cdot \mathbf{r}) \times [1 + \xi^{(2)} \exp(-i2\pi \mathbf{h} \cdot \mathbf{r})]$$

in the substrate ($t<z$)
$$D = D_o^{(s)} \exp[-i2\pi \mathbf{K}_o^{(s)} \cdot (\mathbf{r} - t\mathbf{n})] \times \{1 + \xi^{(s)} \exp[-i2\pi \mathbf{h}^{(s)} \cdot (\mathbf{r} - t\mathbf{n})]\},$$

where the superscript (a) indicates quantities associated with the vacuum and (s) with the substrate. Unmarked symbols are associated with the film and the superscripts (1) and (2) are related respectively to the two wavefields in the film. $\mathbf{K}_o$

represents the incident wavevectors and $\mathbf{K}_h = \mathbf{K}_o + \mathbf{h}$ the reflected ones. D_o is the transmitted beam amplitude and ξ the complex amplitude ratio between the reflected and transmitted beams for each wavefield. For the sake of simplicity, the amplitude of the incident beam $D_o^{(a)}$ is put to 1.

The continuity for the tangential component of the wavevectors on the surface determines the wavevectors $\mathbf{K}_o^{(1,2)}$ and the ratio $\xi^{(1,2)}$ in the film:

$$\mathbf{K}_o^{(1,2)} = \mathbf{K}_o^{(a)} + k\chi_o/2\sin\theta_B\mathbf{n} - [\eta \pm (\eta^2 - 1)^{1/2}]/2\Lambda\mathbf{n}$$

and

$$\xi^{(1,2)} = -(\chi_h\chi_{\bar{h}})^{1/2}/\chi_{\bar{h}}[\eta \pm (\eta^2 - 1)^{1/2}],$$

where upper and lower signs are for wavefields 1 and 2, respectively. k is the magnitude of the incident wavevector $\mathbf{K}_o^{(a)}$. Similar quantities for the wavefield in the substrate, $\mathbf{K}_o^{(s)}$ and $\xi^{(s)}$, are obtained with the same relationships as used for the corresponding substrate parameters. The incidence deviation for the substrate $\eta^{(s)}$ should be set with respect to the substrate Bragg angle. Of the two solutions, only the wavefield with the energy flux directed inwards should be chosen for the substrate.

The amplitudes of the wavefields in the film are determined from the continuity of the dielectric displacements on the surface and interface. This leads to

$$D_o^{(1)} = [\xi^{(s)} - \xi^{(2)}]\exp[-i2\pi t\mathbf{K}_o^{(2)}\cdot\mathbf{n}]/\Delta$$

and

$$D_o^{(2)} = -[\xi^{(s)} - \xi^{(1)}]\exp[-i2\pi t\mathbf{K}_o^{(1)}\cdot\mathbf{n}]/\Delta$$

with

$$\Delta = [\xi^{(s)} - \xi^{(2)}]\exp[-i2\pi t\mathbf{K}_o^{(2)}\cdot\mathbf{n}] - [\xi^{(s)} - \xi^{(1)}]\exp[-i2\pi t\mathbf{K}_o^{(1)}\cdot\mathbf{n}].$$

Thus, the reflectivity of the thin film is obtained by summing the amplitudes of the reflected beams on the surface:

$$R = |D_h^{(a)}|^2 = |D_o^{(1)}\xi^{(1)} + D_o^{(2)}\xi^{(2)}|^2.$$

The X-ray field in the film for any incidence and depth is given by

$$D(z,\eta) = D_o(z,\eta)[1 + \xi(z,\eta)\exp(-i2\pi\mathbf{h}\cdot\mathbf{r})].$$

The values for the transmitted and reflected beams are

$$D_o(z,\eta) = D_o^{(1)}\exp[-i2\pi z\mathbf{K}_o^{(1)}\cdot\mathbf{n}] + D_o^{(2)}\exp[-i2\pi z\mathbf{K}_o^{(2)}\cdot\mathbf{n}]$$
$$D_h(z,\eta) = D_o^{(1)}\xi^{(1)}\exp[-i2\pi z\mathbf{K}_o^{(1)}\cdot\mathbf{n}] + D_o^{(2)}\xi^{(2)}\exp[-i2\pi z\mathbf{K}_o^{(2)}\cdot\mathbf{n}]$$

and the amplitude ratio is defined by $D_h(z,\eta)/D_o(z,\eta)$. It should be noted that these relationships are applicable to the whole angular range from the thin-film reflection to the substrate one. They also allow one to establish the XSW in the substrate under the substrate Bragg reflection with the corresponding characteristics of the wavefield in the substrate: $\mathbf{K}_o^{(s)}$, $D_o^{(s)}$ and $\xi^{(s)}$. The last formulation should be used for the substrate instead of equation (2) when the film reflection is close to the substrate one.

The authors thank Mr Y. Bernard and Mrs D. Demaille for their assistance for the PLD growth. Dr J. Perrière from the GPS (Universities Paris 6 and Paris 7 and CNRS, France) is acknowledged for the RBS calibration, which is essential for the film growth. The authors greatly appreciate the support and advice on the PLD growth from Mr C. Belouet (Alcatel, France). Acknowledgment also goes to Mr M. Morand for the technical improvements of the XSW experimental set-up.

References

Abruña, H. D., Bommarito, G. M. & Acevedo, D. (1990). *Science*, **250**, 69–71.
Albertsson, J., Abrahams, S. C. & Kvick, Å. (1989). *Acta Cryst.* B**45**, 34–40.
Andersen, S. K., Golovchenko, J. A. & Mair, G. (1976). *Phys. Rev. Lett.* **37**, 1141–1145.
Authier, A. (1986). *Acta Cryst.* A**42**, 414–426.
Authier, A., Gronkowski, J. & Malgrange, C. (1989). *Acta Cryst.* A**45**, 432–441.
Batterman, B. W. (1964). *Phys. Rev.* **133**, A759–A764.
Batterman, B. W. (1969). *Phys. Rev. Lett.* **22**, 703–705.
Bedzyk, M. J., Bommarito, G. M., Caffrey, M. & Penner, T. L. (1990). *Science*, **248**, 52–56.
Bedzyk, M. J., Kazimirov, A., Marasco, D. L., Lee, T. L. Foster, C. M., Bai, G. R., Lyman, P. F. & Keane, D. T. (2000). *Phys. Rev. B*, **61**, R7873–7876.
Bensoussan, S., Malgrange, C. & Sauvage-Simkin, M. (1987). *J. Appl. Cryst.* **20**, 222–229.
Boulliard, J. C., Capelle, B., Ferret, D., Lifchitz, A., Malgrange, C., Pétroff, J. F., Taccoen, A. & Zheng, Y. (1992). *J. Phys. (Paris) I*, **2**, 1215–1232.
Chambers, S. A., Droubay, T., Wang, C. M., Lea, A. S., Farrow, R. F. C., Folks, L., Deline, V. & Anders, S. (2003). *Appl. Phys. Lett.* **82**, 1257–1259.
Cowan, P. L., Golovchenko, J. A. & Robbins, M. F. (1980). *Phys. Rev. Lett.* **44**, 1680–1683.
Dietl, T., Ohno, H., Matsukura, F., Cibert, J. & Ferrand, D. (2000). *Science*, **287**, 1019–1022.
Estop, E., Izrael, A. & Sauvage, M. (1976). *Acta Cryst.* A**32**, 627–630.
Fukumura, T., Jin, Z., Ohtomo, A., Koinuma, H. & Kawasaki, M. (1999). *Appl. Phys. Lett.* **75**, 3366–3368.
Golovchenko, J. A., Batterman, B. W. & Brown, W. L. (1974). *Phys. Rev. B*, **10**, 4239–4243.
Henein, G. E. & Wagner, W. R. (1983). *J. Appl. Phys.* **54**, 6395–6400.
Hertel, N., Materlik, G. & Zegenhagen, J. (1985). *Z. Phys.* B**58**, 199–204.
Jedrecy, N., von Bardeleben, H. J., Zheng, Y. & Cantin, J. L. (2004). *Phys. Rev. B*, **69**, R041308-1–R041308-4.
Kato, N. (1998). *Acta Cryst.* A**54**, 203–213.
Kazimirov, A., Haage, T., Ortega, L., Stierle, A., Comin, F. & Zegenhagen, J. (1997). *Solid State Commun.* **104**, 347–350.
Kazimirov, A., Scherb, G., Zegenhagen, J., Lee, T. L., Bedzyk, M. J., Kelly, M. K., Angerer, H. & Ambacher, O. (1998). *J. Appl. Phys.* **84**, 1703–1705.
Kim, J. Y., Park, J. H., Park, B. G., Noh, H. J., Oh, S. J., Yang, J. S., Kim, D. H., Bu, S. D., Noh, T. W., Lin, H. J., Hsieh, H. H. & Chen, C. T. (2003). *Phys. Rev. Lett.* **90**, 017401-1–017401-4.
Koëbel, A., Zheng, Y., Pétroff, J. F., Boulliard, J. C., Capelle, B. & Eddrief, M. (1997). *Phys. Rev. B*, **56**, 12296–12302.
Kohn, V. G. (2002). *Phys. Status Solidi B*, **231**, 132–148.
Lovergine, N., Liacia, L., Ganike, J. D., Leo, G., Drigo, A. V., Romanato, F., Mancini, A. M. & Vasanelli, L. (1995). *J. Appl. Phys.* **78**, 229–235.

Marasco, D. L., Kazimirov, A., Bedzyk, M. J., Lee, T. L., Streiffer, S. K., Auciello, O. & Bai, G. R. (2001). *Appl. Phys. Lett.* **79**, 515–517.
Materlik, G. & Zegenhagen, J. (1984). *J. Phys. Lett.* A**104**, 47–50.
Olego, D. J., Shahzad, K., Petruzzello, J. & Cammack, D. (1987). *Phys. Rev. B*, **36**, 7674–7677.
Patel, J. R. & Golovchenko, J. A. (1983). *Phys. Rev. Lett.* **50**, 1858–1861.
Rozgonyi, G. A. & Ciesielka, T. J. (1973). *Rev. Sci. Instrum.* **44**, 1053–1057.
Saeki, H., Tabata, H. & Kawai, T. (2001). *Solid State Commun.* **120**, 439–443.
Soyer, A. (1995). *J. Appl. Cryst.* **28**, 244.
Ueda, K., Tabata, H. & Kawai, T. (2001). *Appl. Phys. Lett.* **79**, 988–990.
Wang, J., Bedzyk, M. J., Penner, T. L. & Caffrey, M. (1991). *Nature (London)*, **354**, 377–380.
Zegenhagen, J. (1993). *Surf. Sci. Rep.* **18**, 199–271.
Zegenhagen, J., Huang, K. G., Gibson W. M., Hunt, B. D. & Schowalter, L. J. (1989). *Phys. Rev. B*, **39**, 10254–10260.
Zegenhagen, J., Materlik, G. & Uelhoff, W. (1990). *J. X-ray Sci. Technol.* **2**, 214–239.
Zegenhagen, J., Siegrist, T., Fontes, E., Berman, L. E. & Patel, J. R. (1995). *Solid State Commun.* **93**, 763–767.
Zheng, Y., Boulliard, J. C., Demaille, D., Bernard, Y. & Pétroff, J. F. (2004). In preparation.